Label-free characterisation of amyloids and alpha-Synuclein polymorphs by exploiting their intrinsic fluorescence property

Chyi Wei Chung[a+], Amberley D. Stephens[a+], Edward Ward[a], Yuqing Feng[a], Molly Jo Davis[a], Clemens F. Kaminski[a] & Gabriele S. Kaminski Schierle[a*]

[a] Department of Chemical Engineering and Biotechnology, Phillipa Fawcett Drive, University of Cambridge, CB3 0AS.

[+] These authors contributed equally.

[*]Corresponding author: gsk20@cam.ac.uk

Abstract

Conventional *in vitro* aggregation assays often involve tagging with extrinsic fluorophores which can interfere with aggregation. We propose the use of intrinsic amyloid fluorescence lifetime represented by model-free phasor plots, as a label-free assay to characterise amyloid structure. Intrinsic amyloid fluorescence arises from structured packing of β-sheets in amyloids and is independent of aromatic-based fluorescence. We show that different amyloids (i.e., α-Synuclein (αS), β-Lactoglobulin and TasA) and different polymorphic populations of αS (induced by aggregation in salt-free and salt buffers mimicking the intra-/extracellular environments) can be differentiated by their unique fluorescence lifetimes. Moreover, we observe that disaggregation of pre-formed fibrils of αS and βLG leads to increased fluorescence lifetimes, distinct to those of their fibrillar counterpart. Our assay presents a medium-throughput method for rapid classification of amyloids and their polymorphs (the latter of which recent studies have shown lead to different disease pathology), and for testing small molecule inhibitory compounds.

Introduction

Amyloid proteins aggregates share common characteristics, including a fibrillar morphology and cross-β sheet structure.[1] The majority of *in vitro* studies on the kinetics of amyloid aggregation are fluorescence-based using extrinsic fluorophores with a fluorescence intensity readout, yet this presents issues when investigating small molecule inhibitors or fibril polymorphs (i.e., fibrils of different structures within the same amyloid species). Initially developed for histological stains of amyloid plaques in autopsies, common extrinsic fluorophores include Congo Red (CR) and Thioflavin T (ThT) which bind by intercalating between β-sheets of the amyloid of interest.[2] Upon imaging in polarised light, CR-stained amyloids are revealed by apple-green birefringence; whereas increases in fluorescence intensity and quantum yield of ThT are observed with aggregation. However, the binding of both CR and ThT are affected by pH and ionic concentrations, [3,4] which must be strictly controlled under laboratory conditions. ThT based fluorescence assays can be affected by the binding of small inhibitory molecules; hence resulting in interference of fluorescence readings, due to either quenching effects between the molecule and ThT, or competitive binding to active sites on the amyloid protein.[5] Furthermore, the presence of different disease-associated mutants of the Parkinson's disease-related protein α-Synuclein (αS) leads to different ThT binding sites in its fibril polymorphs, and subsequently differences in ThT fluorescence intensity.[6] Tagging recombinant proteins with fluorescent proteins or small dye-labels are also popular methods to study protein aggregation. Yet, the fluorescent protein tag can interfere with the excitation and emission of the ThT fluorescence[7] and large fluorescent proteins can disrupt intramolecular bonding, sterically hinder interactions, and hence alter aggregation rates.[8] As shown in a recent publication, even the presence of small dye

molecules can influence the monomer incorporation into growing amyloid fibrils, thereby yielding polymorphic structures.[9]

Hence, there is motivation for the characterisation of amyloid protein fibrils in a label-free manner, which can be used to investigate potential inhibitors of amyloid aggregation and structural changes to the amyloids. In our previous work, we reported the phenomena of intrinsic amyloid fluorescence,[5,10–12] as corroborated by similar studies from others.[13,14] Characteristically, amyloid fibrils absorb light at wavelengths in the near UV range between 340 – 380 nm and emit fluorescence in the visible range between 400 – 450 nm. This phenomenon is believed to be caused by electron delocalisation due to the rich hydrogen bonding networks between and within the layers of β-sheets comprising an amyloid protein, along with the presence of short hydrogen bonds, resulting in the visible range emission upon UV excitation.[10,11] It is noted that this phenomena is independent of intrinsic aromatic fluorescence as observed with aromatic amino acids (e.g., tyrosine and tryptophan) which exhibit both excitation and emission in the 260 – 280 nm UV range. Amyloid fibrils devoid of aromatic residues still show intrinsic non-aromatic fluorescence in the visible range upon UV excitation.[12,14]

Here, we explore the use of intrinsic amyloid fluorescence lifetime as a potential read out for aggregation states. We choose fluorescence lifetime over fluorescence intensity, as the first is a ratiometric parameter that is independent of excitation intensity, laser scattering, sample concentration and thickness.[15] Several amyloids associated with neurodegenerative diseases feature fluorescence lifetimes in the nanosecond range, with measurements that dispute whether these are mono- or complex exponential in nature.[12,16] Optimal excitation of amyloids is around 350 – 370 nm,[13] wavelengths at which the power density of pulsed supercontinuum sources are very low. The alternative use of two-photon (2P) excitation which involves the absorption of two photons at twice the wavelength but half the energy,[17] has inherent advantages. In contrast to single photon excitation which occurs through a cone of light down to the focal spot within a sample, 2P excitation (and hence any incurred photodamage) is primarily localised to the focal spot.[17,18] This allows for imaging without a pinhole and is more suited for dimmer samples (e.g., intrinsic amyloid fluorescence) as no photons would be rejected due to the lack of a pinhole. The low scattering property of 2P makes it suitable for deeper penetration into samples. The most common implementation involves a femtosecond titanium-sapphire (Ti:S) laser such as the one used in this work, thereby making the technique proposed more accessible for researchers as the setup is commonly available on existing 2P microscopes primarily used for deep tissue imaging.[19–22] Hence, we perform time-correlated single photon counting (TCSPC-) fluorescence lifetime imaging microscopy (FLIM), using 2P excitation. Moreover, we represent 2P-FLIM data on phasor plots, a global analysis approach that is efficient and parameter-free.[23–25] This involves the conversion time-domain TCSPC data into the frequency domain *via* a Fourier transform, thereby giving 'phasors' on a polar plot. This avoids pixel-by-pixel fitting of exponential decays (i.e., a requisite of conventional exponential fitting methods), therefore is highly efficiently and less computationally expensive. Moreover, mono- and complex exponential decay lifetimes can easily be distinguished based on their positions on the phasor plot.

To determine whether 2P-FLIM can differentiate between different amyloids, we used three model amyloids, e.g., β-lactoglobulin (βLG, a globular whey protein) TasA (a functional bacterial amyloid from *Bacillus subtilis*) and αS (the aggregation of which is a hallmark of Parkinson's disease). We observe that they each have unique intrinsic fluorescence lifetimes, which can be used to distinguish between them. We validate our novel fluorescence lifetime

measurements using circular dichroism (CD, which permits the analysis of protein secondary structure) and atomic force microscopy (AFM, which permits the characterisation of individual fibrils). In the amyloid field, the discovery of different fibril strain polymorphs is associated to different toxicity to cells,[26] and potentially different disease outcomes. Hence, in order to better elucidate the pathology of amyloid misfolding diseases, it is useful to efficiently identify different fibril polymorphs.[27,28] Currently, the best method to distinguish between these is cryogenic electron microscopy (cryoEM) due to its high resolution, yet it is a technique that not all researchers have access to and is expensive and low throughput. In the case of αS, we show different distributions of fibril polymorphs are formed in 'no salt' and 'salt' (i.e., mimicking the physiological environment in cells) conditions, which can be distinguished using 2P-FLIM measurements. We further show an increase fluorescence lifetime when the amyloid proteins are disaggregated, indicating structural changes to the amyloids leads to changes in fluorescence lifetime that can be tracked. We therefore provide a cheaper and higher-throughput technique to identify different amyloid fibrils.

Results

Amyloid species can be distinguished by their unique fluorescence lifetimes

We initially performed structural and optical characterisation of the three fibrillar proteins of interest (**Figure 1**). Firstly, we used CD to determine the secondary structure of proteins. The method measures changes in the ellipticity of circularly polarised light when absorbed by different secondary structures (e.g., β-sheet, α-helix) of the protein. We observe that αS (pink) has the highest proportion of β-sheets (i.e., lowest mean residue ellipticity ~ 220 nm) compared to both βLG (blue) and TasA (magenta) (**Figure 1a**). Monomeric αS is intrinsically disordered, but it undergoes structural alteration to β-sheets upon fibrillisation.[29] On the other hand, βLG and TasA both contain β-sheets and α-helices in their monomeric form; both proteins have a decrease in α-helices and an increase in inter-molecular β-sheets upon aggregation.[30,31] In order to perform physical characterisation on single fibrils we used AFM to analyse fibril morphology (**Figure 1b** and **Supplementary Figure 2**). From comparing height profiles, TasA fibrils are evidently shorter in height at 1.0±0.3 nm and without distinctive pitches, in comparison to βLG and αS, with average height profiles of 9.5±3.6 nm and 9.0±3.2 nm, respectively. For βLG and αS, there is a relatively large spread in the height of fibrils formed, which indicates the heterogeneity that exists within the same species sample. Single photon spectrofluorometric measurements reveal that the intrinsic fluorescence for each different amyloid has different optimal excitation and emissions wavelengths in the near UV and visible range respectively (βLG – ex 360 nm, em 430 nm, TasA – ex 350 nm, em 435 nm, and αS – 380 nm, em 425 nm, **Figure 1c**) and this suggests that they can be excited by 2P.

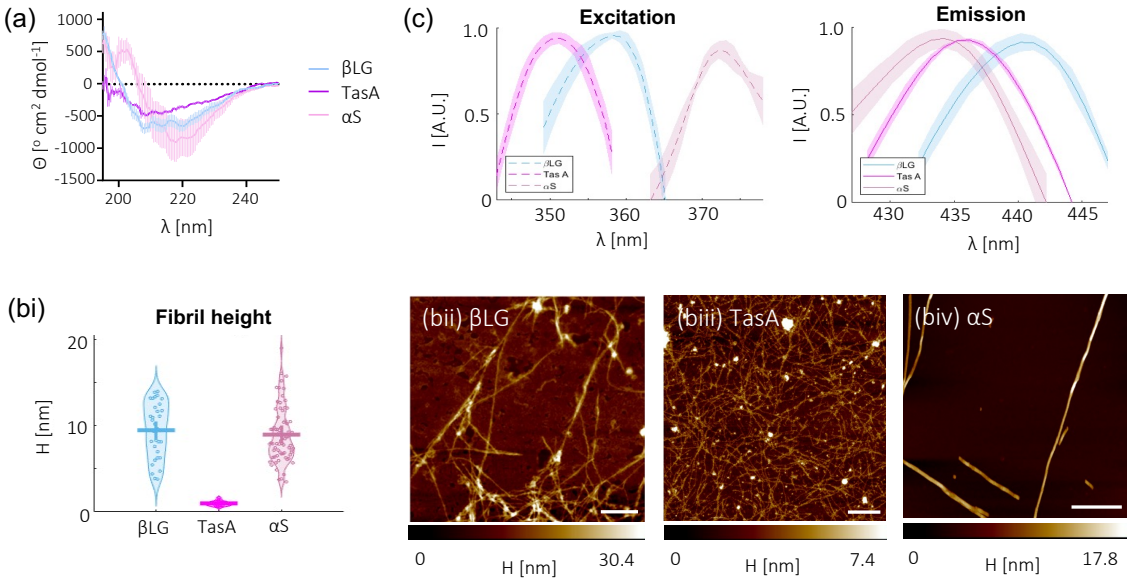

Figure 1: Different amyloid species can be differentiated by their spectral signatures. *(a) CD spectra, displayed as mean ellipticity per residue (Θ), show that aS (pink) has a higher β-sheet content than βLG (blue) and TasA (magenta). Displayed are the average of 10 scans from three individual protein preparations. (b) Representative AFM images show the resulting amyloid fibrils have different morphologies. A height quantification is given in (bi). (bii) βLG fibrils in H_2O are on average 9.5±3.6 nm in height (quoted as mean ± SD). (biii) TasA fibrils in 10 mM Tris pH 8 have no periodicity and are on average 1.0±0.3 nm in height. (biv) aS fibrils in 10 mM Tris pH 7.4 have mixed polymorphs with some fibrils displaying periodicity and others not. Their average height is 9.0±3.2 nm. The height profiles of a total of 33, 15 & 71 fibrils are analysed for βLG, TasA and aS respectively, based on 3 individual protein preparations. Additional AFM images are given in* **Supplementary Figure 2**. *(c) Excitation and emission spectra are measured between 340 to 400 nm with the emission set at peak emission, and emission spectra are measured between 400 to 460 nm with the excitation set at peak excitation for each protein. Excitation and emission peaks for each protein are, βLG – ex 360 nm, em 430 nm, TasA – ex 350 nm, em 435 nm, and aS – 380 nm, em 425 nm. Displayed are the average of three scans from three individual protein preparations.*

We next investigated the intrinsic fluorescence lifetime signatures of the three amyloid fibril samples using 2P-FLIM. We also image the sample topography with AFM, as the diffraction limit on our 2P-FLIM system does not permit the visualisation of small fibrils. We deposit fibrils washed in dH_2O at 100 μM onto clean glass coverslips which are then dried before imaging to provide a dense coverage of protein (**Figure 2a, AFM**). The lifetime of the intrinsic fluorescence emission reveal that all amyloids possess complex exponential with phasors that fall within the universal semicircle (i.e., which denotes mono-exponential lifetimes) of the phasor plot (**Figure 2b**) and in distinct positions from one another. Moreover, there are significant differences in their modulation (τ_M) and phase (τ_φ) lifetimes; for comparison of fluorescence lifetime, τ_M will be quoted henceforth as it is more sensitive than τ_φ. (For an introduction to phasor plot analysis, see **Supplementary Materials**). We measure that βLG has the highest fluorescence lifetime at 1.7±0.2 ns, in comparison to TasA (0.96±0.02 ns) and αS (1.1±0.1 ns) (**Figure 2c**). We note that monomeric fluorescence is too weak to be detected on our 2P-FLIM system.

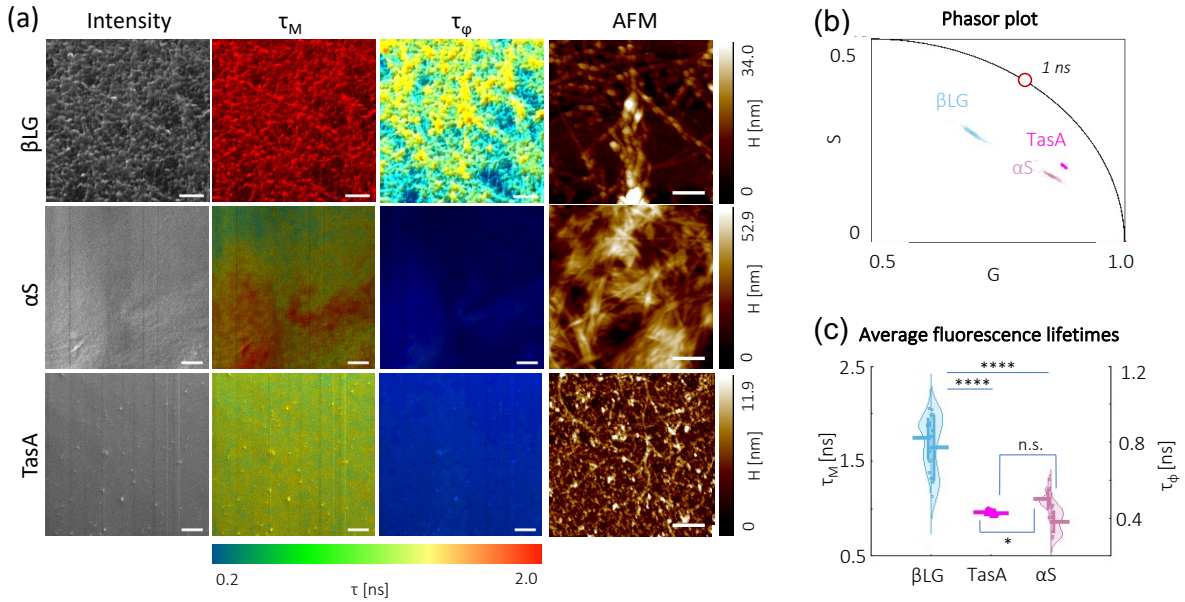

Figure 2: βLG, TasA and αS display different intrinsic fluorescent lifetime signatures. *(a) Fluorescence intensity, fluorescence lifetime (i.e., both modulation τ_M and phase τ_φ) and AFM representative images are shown. Their fluorescence lifetimes follow a multi-exponential decay, as seen from the differences in calculated τ_M and τ_φ (denoting that these phasors lie within the universal semicircle). Scale bars, 10 μm (FLIM) and 400 nm (AFM). (b,c) Phasor plots and average calculated fluorescence lifetimes which show that each amyloid has a distinctive lifetime, but that of βLG is significantly higher. Analysis is based on 10-12 images taken over 3 individual protein preparations. One-way ANOVA test (Holm-Sidak's multiple comparison) where n.s. is not significant, * is $p<0.05$, and **** is $p<0.0001$.*

Salt-aggregated polymorphic populations of αS have quenched fluorescence lifetimes

It has been suggested that structurally different αS fibril polymorphs can lead to different synucleopathies, due to differences in membrane binding, seeding behaviour and toxicity.[32–34] Results in **Figure 2** clearly show that different amyloids can be distinguished by their fluorescence lifetime signatures. Hence, this encouraged us to investigate if fluorescence lifetime is also responsive to more subtle structural changes, e.g., polymorphic variants that emerge for the same protein when aggregated under different buffer conditions. It has previously been shown that 'no salt' and 'salt' aggregation buffer conditions induce the formation of mixed populations of αS polymorphs, where fibrils formed in high salt conditions have distinct periodic pitches instead of flat ribbon structures.[35] Our 'no salt' condition contains 10 mM Tris pH 7.4 (denoted as Tris) and two 'salt' conditions features the addition of 2 mM $CaCl_2$ and 140 mM NaCl ($CaCl_2$/NaCl, i.e., extracellular-mimicking) and 140 mM KCl (KCl, i.e., intracellular-mimicking). 2P-FLIM measurements show lowered fluorescence lifetimes for αS fibrils formed in KCl (0.95±0.09 ns) or $CaCl_2$/NaCl salts (0.96±0.05 ns) compared to αS when aggregated in just Tris buffer (1.1±0.1 ns) (**Figure 3**). Although the magnitude of difference is slight compared to those between different amyloid species (**Figure 2**), this is as expected as there are less structural and molecular packing differences between the αS samples than between differing proteins. Moreover, their fluorescence spectra (**Supplementary Figure 3**) also show similar optimal excitation and emission wavelength.

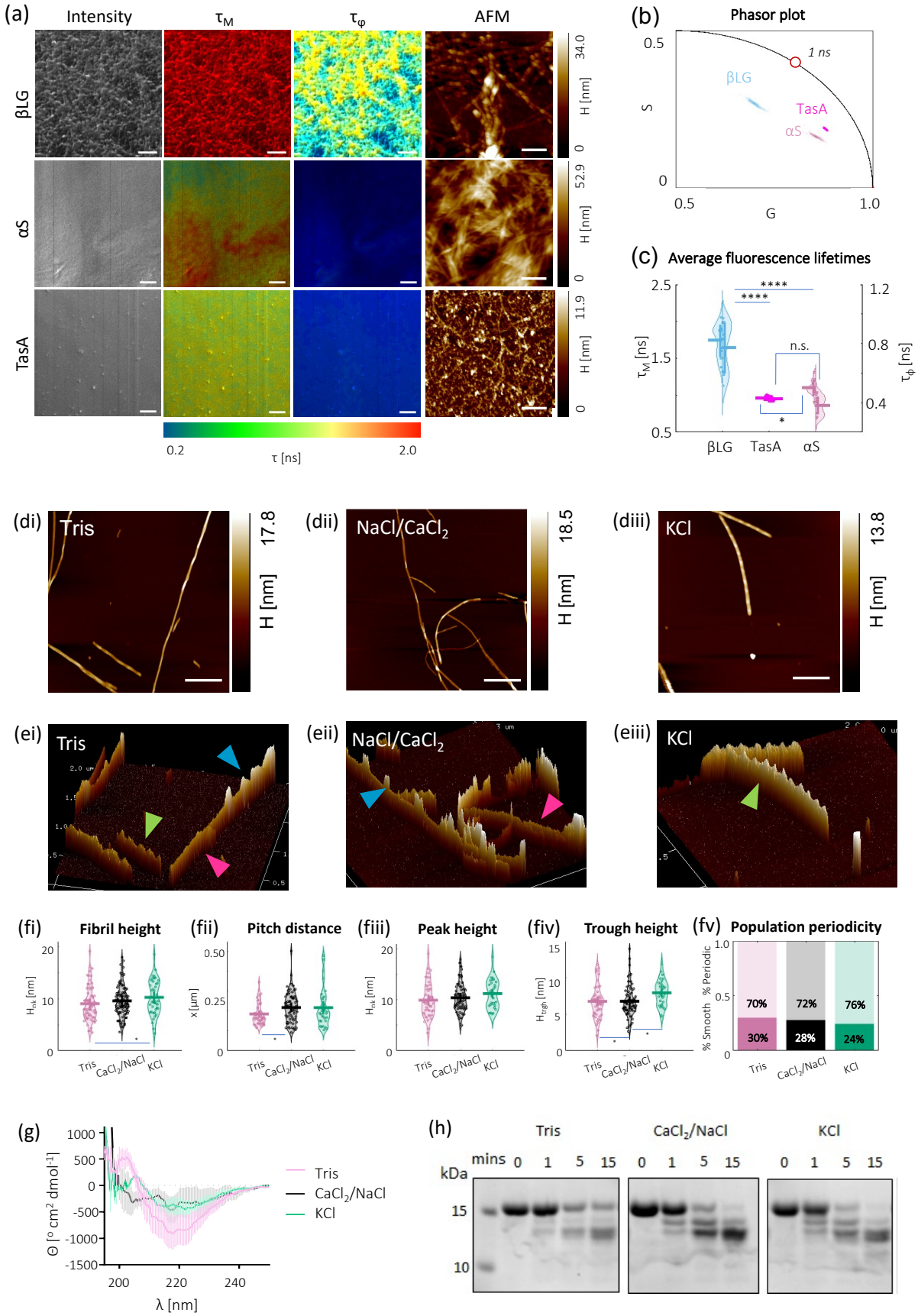
(a)
Intensity
τM
τφ
AFM
βLG
αS
TasA
34.0
52.9
11.9
H [nm]
0.2
τ [ns]
2.0
(b)
Phasor plot
1 ns
βLG
TasA
αS
S
G
0.5
1.0
(c)
Average fluorescence lifetimes
****
n.s.
τM [ns]
τφ [ns]
βLG
TasA
αS
(di)
Tris
17.8
(dii)
NaCl/CaCl2
18.5
(diii)
KCl
13.8
(ei)
(eii)
(eiii)
(fi)
Fibril height
(fii)
Pitch distance
(fiii)
Peak height
(fiv)
Trough height
(fv)
Population periodicity
% Smooth
% Periodic
70%
30%
72%
28%
76%
24%
(g)
Θ [° cm2 dmol-1]
λ [nm]
Tris
CaCl2/NaCl
KCl
(h)
mins
kDa
15
10

Figure 3: αS aggregated in salt buffers exhibit lower fluorescence lifetimes due to variation in the distribution of their polymorphs. (*a) Fluorescence intensity, fluorescence lifetime (i.e., both modulation τ_M and phase τ_φ) and AFM representatives are shown for αS fibrils formed in 20 mM Tris pH 7.4 (Tris), with 1 mM $CaCl_2$ and 140 mM NaCl ($CaCl_2$/NaCl), and with 140 mM KCl (KCl). Scale bars, 10 μm (FLIM) and 400 nm (AFM). (b,c) Phasor plots and average calculated fluorescence lifetimes which show that αS fibrils formed in salts have a lower average fluorescence lifetime compared to those formed in Tris only buffer. Analysis is based on 12 images taken over 3 individual protein preparations. One-way ANOVA test (Holm-Sidak's multiple comparison) where n.s. is not significant, * is p<0.05, * is p<0.001, and **** is p<0.0001. (d) Shown are AFM images of individual fibrils in different buffers for morphological analysis. (e) 3D representations are shown to highlight structural differences. Different morphologies are indicated by coloured arrows, i.e., flat (pink), twisted periodic, from intertwined fibrils (blue) and periodic (green). Additional AFM images are given in* **Supplementary Figure 4.** *(f) Quantification of fibrils shows that there is great heterogeneity within each sample. In general, fibrils aggregated in salt buffers are higher with a lower frequency of pitches. The addition of salts slightly increases the chance of periodic fibrils over flat ones. The height profiles of a total of 71, 97 & 47 fibrils are analysed for αS aggregated in Tris, $CaCl_2$/NaCl and KCl, respectively, based on 3 protein preparations. One-way ANOVA test (Holm-Sidak's multiple comparison) where ns is not significant, * is p<0.05, * is p<0.001, and **** is p<0.0001. (g) CD of 2.5 μM of each protein fibrils show that αS in Tris has a higher β-sheet content compared to αS in 140 mM KCl and 140 mM NaCl and $CaCl_2$. 10 scans of each sample were taken, and the average is shown for three protein sample preparations, with buffer only signals subtracted (h) 100 μM of αS in each buffer condition was incubated in proteinase K for 0, 1, 5 and 15 mins. Monomeric αS has a molecular weight of ~14.4 kDa, degradation patterns of the three samples show a similar band profile, but the intensities differ, indicating differences in cleavage rates. A second repeat is shown in* **Supplementary Figure 5** *with similar proteolysis profiles.*

We then further characterise the three αS fibril samples to determine whether they are truly structurally and/or morphologically different. 2D and 3D AFM images show several different αS fibril polymorphs within each buffer condition (**Figure 3d-e** and **Supplementary Figure 4**), these polymorphs can be classified as either smooth (pink arrows), periodic (green arrows) or twisted periodic, likely arising from two fibrils twisting around each other (blue arrows). We performed single fibril analysis based on AFM images, to classify the height distribution and the prevalence of periodicity within each sample. As before, we observe a wide range of heights from fibrils within the same sample, with an average height of 9.0±3.2 nm (Tris), 9.6±2.9 nm ($CaCl_2$/NaCl), and 10.2±3.3 nm (KCl) (**Figure 3fi**). The addition of salts promotes the formation of higher and intertwined fibrils, of which there is a greater proportion of those being periodic (i.e., 72% & 76% for $CaCl_2$/NaCl and KCl, respectively in comparison to 70% for Tris, **Figure 3fv**). This is most apparent in the αS fibrils formed in KCl, where the fibril height distribution is more bimodal, showing single fibril height and double fibril height (**Figure 3fi**).

CD measurements show that αS aggregated in salt buffers have a decreased β-sheet content compared to those in Tris (**Figure 3g**). Furthermore, differences in fibril proteolysis profiles can be used to indicate a different fibril structure and core due to differences in accessibility of the protease.[36] Limited proteolysis of the αS fibrils in the three buffers with proteinase K shows similar digestion profiles, but differing band intensity, indicating similarities in core structure, but differences in fibril packing and accessibility of proteinase K to the cleavage sites in the different fibril samples (**Figure 3h**, with a repeat shown in **Supplementary Figure 5**). Therefore, our sample characterisation supports structural differences in the fibrils formed under different salt conditions which we observe to possess different fluorescence lifetimes.

Disaggregation of fibrils increases their fluorescence lifetimes

Lastly, to validate the use of intrinsic fluorescence lifetime as an *in vitro* label-free aggregation assay, we disaggregate fibrillar αS and βLG by mixing the samples with hexafluoro-2-propanol (HFIP), a solvent typically used to monomerise proteins before aggregation. We observe the formation of shortened fibrils and oligomers in αS and βLG, respectively, in AFM images (**Figure 4a**, AFM). Correspondingly, these disaggregated structures lead to significantly increased fluorescence lifetimes, especially in the case of oligomeric βLG (2.6±0.1 ns from 1.7±0.2 ns) and less so for αS (1.2±0.06 ns from 1.1±0.1 ns) (**Figure 4b-c**). As the intrinsic amyloid fluorescence could still be detected from both samples, this insinuates there is still β-sheet stacking present in the disaggregated structures of βLG and αS, yet a change in the stacking or arrangement during partial disaggregation has led to a change in intrinsic fluorescence lifetime.

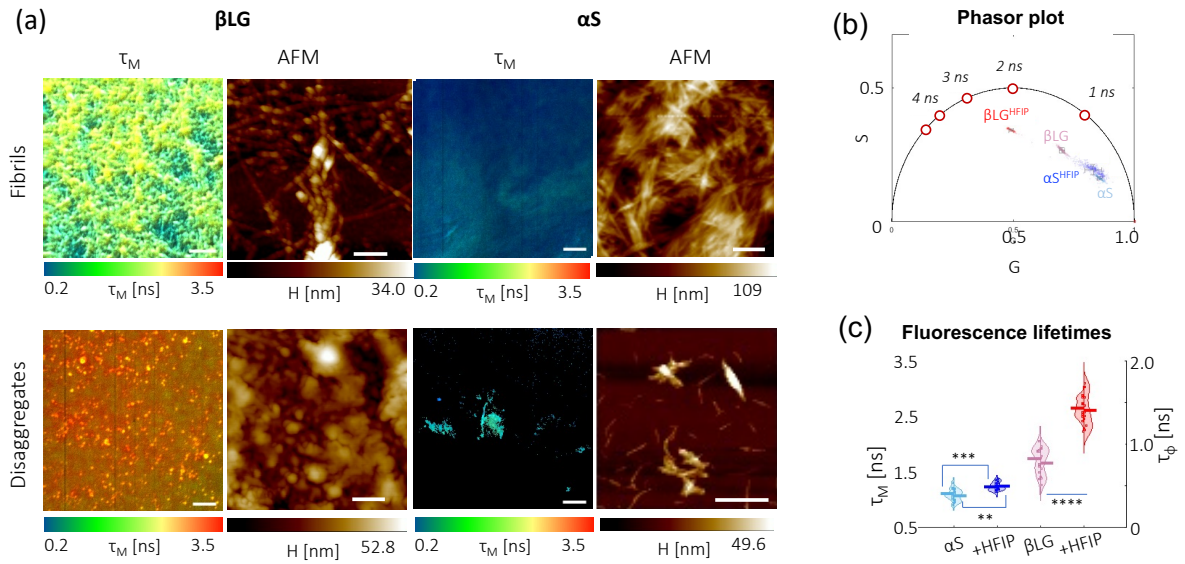

Figure 4: The fluorescence lifetime change of different amyloid proteins upon aggregation is reversible with disaggregated structures of αS and βLG having higher fluorescence lifetimes than their fibrillar counterparts. *(a) Fluorescence lifetimes and AFM images comparing αS and βLG fibrils before and after disaggregation by HFIP. Scale bars, 10 µm (FLIM) and 400 nm (AFM). (b,c,) Phasor plot and average fluorescence lifetimes show a significant decrease in fluorescence lifetime after the addition of HFIP to disaggregate the fibrils for both αS and βLG. One-way ANOVA test (Holm-Sidak's multiple comparison) where n.s. is not significant, * is p<0.05, and **** is p<0.0001.*

Discussion

There is a need for label-free techniques to identify and monitor aggregation of amyloid proteins that is currently unmet. Here, we use a combination of structural and morphological techniques to validate the use of 2P-FLIM in identifying different amyloid protein fibrils, their polymorphs and their disaggregated states using fluorescence lifetime imaging. We investigate three amyloid proteins: βLG, a milk whey protein which is commonly used as a model amyloid protein, as it is inexpensive and readily available; TasA, a functional amyloid of *B. subtilis* involved in adherence and formation of the extracellular scaffold of biofilms; and αS, whose aggregation is a hallmark of synucleinopathies, such as Parkinson's Disease. The fluorescence lifetime of conventional fluorophores, e.g., GFP, are influenced by the surrounding environment.[37,38] The field of intrinsic non-aromatic fluorescence is comparatively young, therefore studies into differences in amyloid structures and interaction with the local environment have not yet been fully conducted yet may well be influenced by fibril packing and environmental interactions, which can lead to unique lifetimes for different proteins and polymorphs. Here, we efficiently represent the unique intrinsic fluorescence lifetime signatures of different amyloids, using model-free phasor plot analysis.

We then investigated whether 2P-FLIM could be used to identify fibril polymorphs of the same protein. The fibril formation of αS is implicated with several neuropathological diseases, including but not limited to, Parkinson's disease, dementia with Lewy bodies, and multiple system atrophy.[39] As aforementioned, cryoEM which boasts of a 3.7 Å resolution,[27,40] is currently the gold standard technique for distinguishing and classifying amyloid (including αS) polymorphs, yet is an expensive technique that requires skilled users.[1] Moreover, cryoEM has low throughput, hence it is unsuited for small molecule screening and cannot be used to investigate changes in protein states as they aggregate or change under different environmental conditions. Here, we use 2P-FLIM and show that αS fibrils formed in salt buffers mimicking the intracellular and extracellular have a slightly quenched fluorescence lifetime compared to the polymorphs formed without salt. From a structural perspective, noting that the fibrils are washed in H_2O prior to 2P-FLIM imaging to remove salt ions, this quenching effect could be attributed to differences in the fibril packing (from limited proteolysis) or β-sheet structure (from CD) leading to the formation of different fibril polymorphs, that appear to have higher fibrils and less frequent pitches (from AFM). While we identify bigger differences between the 'no salt' Tris sample and the salt samples, there is a slight, but insignificant difference in the fluorescence lifetimes which is lower for αS fibrils formed in KCl than in $CaCl_2$/NaCl. The two salt conditions were chosen to mimic intracellular and extracellular conditions, where in the latter calcium concentrations are higher. We, along with others, have previously shown that αS specifically binds calcium at its negatively charged C-terminus, this leads to altered monomeric structures and fibril polymorphs which may be important in cases of αS spreading from neuron to neuron.[41,42] It is not known whether the structures formed *in vitro* are those that are formed *in vivo*,[43] in addition to whether different structures arise when aggregated in the intracellular and extracellular space. Further structural analysis using mutants and computational simulations may be able to pin-point the mechanisms that derive differences in fluorescence lifetime.

To quantify structural differences, we show that disaggregating pre-formed fibrils of αS and βLG result in an increase to their measured fluorescence lifetimes. We believe this stems from the looser packing and reduction β-sheets in within the disaggregated structures (i.e., smaller fibrils for αS and oligomers for βLG).[44]

We validate that intrinsic amyloid fluorescence lifetime can be used as a label-free method to characterise different amyloid proteins, as well as the distribution within polymorphic populations of αS and disaggregated structures. Our current work comprises of observations on intrinsic amyloid fluorescence, which we find is affected by several different factors, e.g., β-sheet content and molecular packing. 2P-FLIM and efficient phasor plot analysis of fluorescence lifetimes maybe useful if applied to drug screening for amyloid protein targeting compounds, as 2P-FLIM can circumvent issues with small molecule interference with fluorescence intensity-based assays. To complement our findings, we believe that computational studies on the molecular structure of these amyloids at an atomistic scale that permit the study of electron transitions would be needed to establish causative links between structure and the unique fluorescence lifetime signatures amyloid possess. In general, intrinsic amyloid fluorescence lifetime in conjunction with fit-free phasor plot analysis provides a medium-throughput, efficient and label-free method to distinguish between different amyloids and their polymorphs.

Acknowledgements

C.W.C. jointly funded by the Cambridge Trust and Wolfson College for her PhD. G.S.K.S. acknowledges funding from the Wellcome Trust (065807/Z/01/Z) (203249/Z/16/Z), the UK Medical Research Council (MRC) (MR/K02292X/1), Alzheimer Research UK (ARUK) (ARUK-PG013-14), Michael J Fox Foundation (16238) and Infinitus China Ltd. M.J.D. was funded by NanoDTC ESPSRC Grant EP/S022953/1. We thank Naunehal Matharu for preliminary CD data not in the final manuscript and Maria Zacharopoulou for discussions on αS fibril polymorphs.

Author contributions

G.S.K.S., C.W.C. and A.D.S conceived the manuscript. C.W.C, A.D.S, Y.F. and M.J.D. prepared protein for experiments. C.W.C. and E.W. built the 2P-FLIM, C.W.C collected 2P-FLIM data, C.W.C analysed 2P-FLIM data. C.W.C. collected excitation and emission spectra. A.D.S. collected CD data. C.W.C and A.D.S. collected AFM data, C.W.C analysed AFM data. A.D.S. performed limited proteolysis. C.F.K. provided equipment. All authors contributed to paper writing. All authors have given approval to the final version of the paper. All raw data is available on request and in the Cambridge University Repository (Apollo ID: A48E00D8-68DB-45B7-A368-406503E36D23). All analysis scripts are available on request.

References

(1) Guerrero-Ferreira, R.; Kovacik, L.; Ni, D.; Stahlberg, H. New Insights on the Structure of Alpha-Synuclein Fibrils Using Cryo-Electron Microscopy. *Curr. Opin. Neurobiol.* **2020**, *61*, 89–95. https://doi.org/10.1016/j.conb.2020.01.014.

(2) Biancalana, M.; Koide, S. Molecular Mechanism of Thioflavin-T Binding to Amyloid Fibrils. *Biochimica et Biophysica Acta - Proteins and Proteomics* **2010**, *1804* (7), 1405–1412. https://doi.org/10.1016/j.bbapap.2010.04.001.

(3) Mikalauskaite, K.; Ziaunys, M.; Sneideris, T.; Smirnovas, V. Effect of Ionic Strength on Thioflavin-T Affinity to Amyloid Fibrils and Its Fluorescence Intensity. *Int. J. Mol. Sci.* **2020**, *21* (23), 8916. https://doi.org/10.3390/ijms21238916.

(4) Hackl, E. v.; Darkwah, J.; Smith, G.; Ermolina, I. Effect of Acidic and Basic PH on Thioflavin T Absorbance and Fluorescence. *Eur. Biophys. J.* **2015**, *44* (4), 249–261. https://doi.org/10.1007/S00249-015-1019-8/TABLES/3.

(5) Pinotsi, D.; Buell, A. K.; Dobson, C. M.; Kaminski Schierle, G. S.; Kaminski, C. F. A Label-Free, Quantitative Assay of Amyloid Fibril Growth Based on Intrinsic Fluorescence. *Chem. Bio. Chem.* **2013**, *14* (7), 846–850. https://doi.org/10.1002/cbic.201300103.

(6) Sidhu, A.; Vaneyck, J.; Blum, C.; Segers-Nolten, I.; Subramaniam, V. Polymorph-Specific Distribution of Binding Sites Determines Thioflavin-T Fluorescence Intensity in α-Synuclein Fibrils. *Amyloid* **2018**, *25* (3), 189–196. https://doi.org/10.1080/13506129.2018.1517736.

(7) Anderson, V. L.; Webb, W. W. Transmission Electron Microscopy Characterization of Fluorescently Labelled Amyloid β 1-40 and α-Synuclein Aggregates. *BMC Biotechnol.* **2011**, *11* (1), 1–10. https://doi.org/10.1186/1472-6750-11-125/FIGURES/6.

(8) Afitska, K.; Fucikova, A.; Shvadchak, V. v.; Yushchenko, D. A. Modification of C Terminus Provides New Insights into the Mechanism of α-Synuclein Aggregation. *Biophys. J.* **2017**, *113* (10), 2182–2191. https://doi.org/10.1016/J.BPJ.2017.08.027.

(9) Cosentino, M.; Canale, C.; Bianchini, P.; Diaspro, A. AFM-STED Correlative Nanoscopy Reveals a Dark Side in Fluorescence Microscopy Imaging. *Sci. Adv.* **2019**, *5* (6), eaav8062. https://doi.org/10.1126/sciadv.aav8062.

(10) Pinotsi, D.; Grisanti, L.; Mahou, P.; Gebauer, R.; Kaminski, C. F.; Hassanali, A.; Kaminski Schierle, G. S. Proton Transfer and Structure-Specific Fluorescence in Hydrogen Bond-Rich Protein Structures. *J. Am. Chem. Soc.* **2016**, *138* (9), 3046–3057. https://doi.org/10.1021/jacs.5b11012.

(11) Stephens, A. D.; Qaisrani, M. N.; Ruggiero, M. T.; Mirón, G. D.; Morzan, U. N.; Lebrero, M. C. G.; Jones, S. T. E.; Poli, E.; Bond, A. D.; Woodhams, P. J.; Kleist, E. M.; Grisanti, L.; Gebauer, R.; Zeitler, J. A.; Credgington, D.; Hassanali, A.; Schierle, G. S. K. Short Hydrogen Bonds Enhance Nonaromatic Protein-Related Fluorescence. *Proc. Natl. Acad. Sci.* **2021**, *118* (21). https://doi.org/10.1073/PNAS.2020389118.

(12) Chan, F. T. S.; Kaminski Schierle, G. S.; Kumita, J. R.; Bertoncini, C. W.; Dobson, C. M.; Kaminski, C. F. Protein Amyloids Develop an Intrinsic Fluorescence Signature during Aggregation. *Analyst* **2013**, *138* (7), 2156–2162. https://doi.org/10.1039/c3an36798c.

(13) Shukla, A.; Mukherjee, S.; Sharma, S.; Agrawal, V.; Kishan, K. V. R.; Guptasarma, P. A Novel UV Laser-Induced Visible Blue Radiation from Protein Crystals and Aggregates: Scattering Artifacts or Fluorescence

Transitions of Peptide Electrons Delocalized through Hydrogen Bonding? *Arch. Biochem. Biophys.* **2004**, *428*, 144–153. https://doi.org/10.1016/j.abb.2004.05.007.

(14) del Mercato, L. L.; Pompa, P. P.; Maruccio, G.; della Torre, A.; Sabella, S.; Tamburro, A. M.; Cingolani, R.; Rinaldi, R. Charge Transport and Intrinsic Fluorescence in Amyloid-like Fibrils. *Proc. Natl. Acad. Sci. U. S. A.* **2007**, *104* (46), 18019–18024. https://doi.org/10.1073/pnas.0702843104.

(15) Becker, W. Fluorescence Lifetime Imaging - Techniques and Applications. *J. Microsc.* **2012**, *247* (2), 119–136. https://doi.org/10.1111/j.1365-2818.2012.03618.x.

(16) Hecker, L.; Wang, W.; Mela, I.; Fathi, S.; Poudel, C.; Soavi, G.; Huang, Y. Y. S.; Kaminski, C. F. Guided Assembly and Patterning of Intrinsically Fluorescent Amyloid Fibers with Long-Range Order. *Nano Lett.* **2021**, *21* (2), 938–945. https://doi.org/10.1021/ACS.NANOLETT.0C03672.

(17) Denk, W.; Strickler, J. H.; Webb, W. W. Two-Photon Laser Scanning Fluorescence Microscopy. *Science* **1990**, *248* (4951), 73–76. https://doi.org/10.1126/SCIENCE.2321027.

(18) Benninger, R. K. P.; Piston, D. W. Two-Photon Excitation Microscopy for the Study of Living Cells and Tissues. *Curr. Protoc. Cell Biol.* **2013**, *59* (1), 4.11.1-4.11.24. https://doi.org/10.1002/0471143030.CB0411S59.

(19) Larson, A. M. Multiphoton Microscopy. *Nat. Photonics* **2010**, *5* (1), 1–1. https://doi.org/10.1038/nphoton.an.2010.2.

(20) Moulton, P. F. Spectroscopic and Laser Characteristics of Ti:Al2O3. *J. Opt. Soc. Am. B* **1986**, *3* (1), 125–133. https://doi.org/10.1364/JOSAB.3.000125.

(21) Svoboda, K.; Yasuda, R. Principles of Two-Photon Excitation Microscopy and Its Applications to Neuroscience. *Neuron* **2006**, *50* (6), 823–839. https://doi.org/10.1016/J.NEURON.2006.05.019.

(22) Miller, D. R.; Jarrett, J. W.; Hassan, A. M.; Dunn, A. K. Deep Tissue Imaging with Multiphoton Fluorescence Microscopy. *Curr. Opin. Biomed. Eng.* **2017**, *4*, 32–39. https://doi.org/10.1016/J.COBME.2017.09.004.

(23) Ranjit, S.; Malacrida, L.; Jameson, D. M.; Gratton, E. Fit-Free Analysis of Fluorescence Lifetime Imaging Data Using the Phasor Approach. *Nat. Protoc.* **2018**, *13* (9), 1979–2004. https://doi.org/10.1038/s41596-018-0026-5.

(24) Liao, S.-C.; Sun, Y.; Coskun, U. *FLIM Analysis Using the Phasor Plots*; Champaign, 2014.

(25) Digman, M. A.; Caiolfa, V. R.; Zamai, M.; Gratton, E. The Phasor Approach to Fluorescence Lifetime Imaging Analysis. *Biophys. J.* **2008**, *94* (2), L14. https://doi.org/10.1529/BIOPHYSJ.107.120154.

(26) Peng, C.; Gathagan, R. J.; Lee, V. M. Y. Distinct α-Synuclein Strains and Implications for Heterogeneity among α-Synucleinopathies. *Neurobiol. Disease* **2018**, *109* (Pt B), 209–218. https://doi.org/10.1016/j.nbd.2017.07.018.

(27) Li, B.; Ge, P.; Murray, K. A.; Sheth, P.; Zhang, M.; Nair, G.; Sawaya, M. R.; Shin, W. S.; Boyer, D. R.; Ye, S.; Eisenberg, D. S.; Zhou, Z. H.; Jiang, L. Cryo-EM of Full-Length α-Synuclein Reveals Fibril Polymorphs with a Common Structural Kernel. *Nat. Commun.* **2018**, *9* (1), 1–10. https://doi.org/10.1038/s41467-018-05971-2.

(28) Guerrero-Ferreira, R.; Kovacik, L.; Ni, D.; Stahlberg, H. New Insights on the Structure of Alpha-Synuclein Fibrils Using Cryo-Electron Microscopy. *Curr. Opin. Neurobiol.* **2020**, *61*, 89–95. https://doi.org/10.1016/j.conb.2020.01.014.

(29) Giasson, B. I.; Murray, I. V. J.; Trojanowski, J. Q.; Lee, V. M. Y. A Hydrophobic Stretch of 12 Amino Acid Residues in the Middle of α-Synuclein Is Essential for Filament Assembly. *J. Biol. Chem.* **2001**, *276* (4), 2380–2386. https://doi.org/10.1074/JBC.M008919200.

(30) Ioannou, J. C.; Donald, A. M.; Tromp, R. H. Characterising the Secondary Structure Changes Occurring in High Density Systems of BLG Dissolved in Aqueous PH 3 Buffer. *Food Hydrocolloids* **2015**, *46*, 216–225. https://doi.org/10.1016/J.FOODHYD.2014.12.027.

(31) Chai, L.; Romero, D.; Kayatekin, C.; Akabayov, B.; Vlamakis, H.; Losick, R.; Kolter, R. Isolation, Characterization, and Aggregation of a Structured Bacterial Matrix Precursor. *J. Biol. Chem.* **2013**, *288* (24), 17559. https://doi.org/10.1074/JBC.M113.453605.

(32) Landureau, M.; Redeker, V.; Bellande, T.; Eyquem, S.; Melki, R. The Differential Solvent Exposure of N-Terminal Residues Provides "Fingerprints" of Alpha-Synuclein Fibrillar Polymorphs. *J. Biol. Chem.* **2021**, *296*. https://doi.org/10.1016/J.JBC.2021.100737.

(33) Meade, R. M.; Williams, R. J.; Mason, J. M. A Series of Helical α-Synuclein Fibril Polymorphs Are Populated in the Presence of Lipid Vesicles. *NPJ Parkinson's Disease* **2020**, *6* (1). https://doi.org/10.1038/s41531-020-00122-1.

(34) de Giorgi, F.; Laferrière, F.; Zinghirino, F.; Faggiani, E.; Lends, A.; Bertoni, M.; Yu, X.; Grélard, A.; Morvan, E.; Habenstein, B.; Dutheil, N.; Doudnikoff, E.; Daniel, J.; Claverol, S.; Qin, C.; Loquet, A.; Bezard, E.; Ichas, F. Novel Self-Replicating α-Synuclein Polymorphs That Escape ThT Monitoring Can Spontaneously Emerge and Acutely Spread in Neurons. *Sci. Adv.* **2020**, *6*, eabc4364.

(35) Gath, J.; Bousset, L.; Habenstein, B.; Melki, R.; Böckmann, A.; Meier, B. H. Unlike Twins: An NMR Comparison of Two α-Synuclein Polymorphs Featuring Different Toxicity. *PLOS ONE* **2014**, *9* (3), e90659. https://doi.org/10.1371/JOURNAL.PONE.0090659.

(36) Landureau, M.; Redeker, V.; Bellande, T.; Eyquem, S.; Melki, R. The Differential Solvent Exposure of N-Terminal Residues Provides "Fingerprints" of Alpha-Synuclein Fibrillar Polymorphs. *J. Biol. Chem.* **2021**, *296*. https://doi.org/10.1016/J.JBC.2021.100737.

(37) Berezin, M. Y.; Achilefu, S. Fluorescence Lifetime Measurements and Biological Imaging. *Chem. Rev.* **2010**, *110* (5), 2641–2684. https://doi.org/10.1021/CR900343Z.

(38) Kafle, B. P. Molecular Luminescence Spectroscopy. *Chem. Anal. Mat. Charac. Spectrophotometry* **2020**, 269–296. https://doi.org/10.1016/B978-0-12-814866-2.00009-9.

(39) Peng, C.; Gathagan, R. J.; Covell, D. J.; Medellin, C.; Stieber, A.; Robinson, J. L.; Zhang, B.; Pitkin, R. M.; Olufemi, M. F.; Luk, K. C.; Trojanowski, J. Q.; Lee, V. M. Y. Cellular Milieu Imparts Distinct Pathological α-Synuclein Strains in α-Synucleinopathies. *Nature 2018 557:7706* **2018**, *557* (7706), 558–563. https://doi.org/10.1038/s41586-018-0104-4.

(40) Guerrero-Ferreira, R.; Taylor, N. M.; Arteni, A.-A.; Kumari, P.; Mona, D.; Ringler, P.; Britschgi, M.; Lauer, M. E.; Makky, A.; Verasdonck, J.; Riek, R.; Melki, R.; Meier, B. H.; Bö ckmann, A.; Bousset, L.; Stahlberg, H. Two New Polymorphic Structures of Human Full-Length Alpha-Synuclein Fibrils Solved by Cryo-Electron Microscopy. *eLife* **2019**, *8*, e48907. https://doi.org/10.7554/eLife.48907.

(41) Lautenschläger, J.; Stephens, A. D.; Fusco, G.; Ströhl, F.; Curry, N.; Zacharopoulou, M.; Michel, C. H.; Laine, R.; Nespovitaya, N.; Fantham, M.; Pinotsi, D.; Zago, W.; Fraser, P.; Tandon, A.; St George-Hyslop, P.; Rees, E.; Phillips, J. J.; de Simone, A.; Kaminski, C. F.; Schierle, G. S. K. C-Terminal Calcium Binding of α-Synuclein Modulates Synaptic Vesicle Interaction. *Nat. Commun.* **2018**, *9* (1), 1–13. https://doi.org/10.1038/s41467-018-03111-4.

(42) Han, J. Y.; Choi, T. S.; Kim, H. I. Molecular Role of Ca2+ and Hard Divalent Metal Cations on Accelerated Fibrillation and Interfibrillar Aggregation of α-Synuclein. *Sci. Rep.* **2018**, *8* (1), 1–11. https://doi.org/10.1038/s41598-018-20320-5.

(43) Lövestam, S.; Schweighauser, M.; Matsubara, T.; Murayama, S.; Tomita, T.; Ando, T.; Hasegawa, K.; Yoshida, M.; Tarutani, A.; Hasegawa, M.; Goedert, M.; Scheres, S. H. W. Seeded Assembly in Vitro Does Not Replicate the Structures of α-Synuclein Filaments from Multiple System Atrophy. *FEBS open bio* **2021**, *11* (4), 999–1013. https://doi.org/10.1002/2211-5463.13110.

(44) Chen, S. W.; Drakulic, S.; Deas, E.; Ouberai, M.; Aprile, F. A.; Arranz, R.; Ness, S.; Roodveldt, C.; Guilliams, T.; De-Genst, E. J.; Klenerman, D.; Wood, N. W.; Knowles, T. P. J.; Alfonso, C.; Rivas, G.; Abramov, A. Y.; Valpuesta, J. M.; Dobson, C. M.; Cremades, N. Structural Characterization of Toxic Oligomers That Are Kinetically Trapped during α-Synuclein Fibril Formation. *Proceed. Natl. Acad. Sci. U.S.A.* **2015**, *112* (16), E1994–E2003. https://doi.org/10.1073/PNAS.1421204112/-/DCSUPPLEMENTAL.

(45) Schlachter, S.; Elder, A. D.; Esposito, A.; Kaminski, G. S.; Frank, J. H.; van Geest, L. K.; Kaminski, C. F.; Matthews, S. M.; Yunus, K.; Brennan, C. M.; Fisher, A. C. MhFLIM: Resolution of Heterogeneous Fluorescence Decays in Widefield Lifetime Microscopy. *Opt. Express* **2009**, *17* (3), 1557–1570. https://doi.org/10.1364/OE.17.001557.

(46) Elder, A. D.; Kaminski, C. F.; Frank, J. H. Φ2FLIM: A Technique for Alias-Free Frequency Domain Fluorescence Lifetime Imaging. *Opt. Express* **2009**, *17* (25), 23181–23203. https://doi.org/10.1364/OE.17.023181.

(47) Stephens, A. D.; Matak-Vinkovic, D.; Fernandez-Villegas, A.; Kaminski Schierle, G. S. Purification of Recombinant α-Synuclein: A Comparison of Commonly Used Protocols. *Biochem.* **2020**, *59* (48), 4563–4572. https://doi.org/10.1021/ACS.BIOCHEM.0C00725/SUPPL_FILE/BI0C00725_SI_001.PDF.

Methods

Purification of αS

Human wild-type (WT) alpha-synuclein (αS) was expressed from plasmid pT7-7. The plasmid was heat shocked into Escherichia coli One Shot® BL21 STAR™ (DE3) (Invitrogen, Thermo Fisher Scientific, Cheshire, UK) and purified as previously described by periplasmic lysis of *E. coli* and chromatographic separation of the proteins.[47] Recombinant αS was purified using ion exchange chromatography (IEX) in buffer A (10 mM Tris, 1 mM EDTA pH 8) against a linear gradient of buffer B (10 mM Tris, 1 mM EDTA, 0.15 M $(NH_4)_2SO_4$ pH 8) on a HiPrep Q FF 16/10 anion exchange column (GE Healthcare, Uppsala, Sweden). The concentration of $(NH_4)_2SO_4$ in the pooled αS fractions was calculated and the equivalent $(NH_4)_2SO_4$ added to make the protein solution to 1 M. αS was then further purified on a HiPrep Phenyl FF 16/10 (High Sub) hydrophobic interaction chromatography (HIC) column (GE Healthcare) in buffer C (1 M $(NH_4)_2SO_4$, 50 mM Bis-Tris pH 7) and eluted against buffer D (50 mM Bis-Tris pH 7). Purification was performed on an ÄKTA Pure (GE Healthcare). αS was concentrated using 10 k MWCO amicon centrifugal filtration devices (Merck KGaA, Darmstadt, Germany) and monomeric αS isolated using a gel filtration HiLoad 16/60 superdex 75 pg column (GE Healthcare) in 20 mM Tris pH 7.4 and stored at −80 °C until use. Protein concentration was determined from the absorbance measurement at 280 nm on a Nanovue spectrometer using the extinction coefficient for αS of 5960 $M^{-1}cm^{-1}$.

Purification of TasA

Bacillus subtilis TasA was expressed using a pET24 plasmid. Residues 1-27, encoding the signal peptide of TasA was not included to permit purification of the mature $TasA^{28-261}$ protein, subsequently referred to as TasA. A 6xHis-tag was situated at the N terminus and a tobacco etch virus (TEV) protease recognition site ENLYFQ/x inserted before the N-terminus of the TasA protein to give the sequence MHHHHHHENLYFQ/F where '/' denotes the TEV cleavage site and F the beginning residue of the mature TasA. pET24:⊿*27tasA* was transformed into *E. coli* BL21 (DE3) pLysS cells which were grown at 37°C with constant shaking at 250 rpm to an optical density at 600 nm of 0.8. Protein expression was induced with 1 mM isopropyl-β-thiogalactopyranoside (IPTG) and grown overnight at 21°C with shaking at 200 rpm. *E. coli* cultures were centrifuged at 8000 rpm for 15 min and the pellet resuspended in 20 mM Tris, pH 8, 0.5 M NaCl, 1 tablet protease inhibitors, 1 mM $MgCl_2$ and sonicated 5 × 30 s on ice. The sonicate was centrifuged at 10,000 rpm, 4°C for 15 min. The supernatant was filtered through a 0.22 um filter and loaded onto a HisTrap Excel 5 mL column (GE Healthcare). The column was equilibrated in buffer A (20 mM Tris, 0.5 M NaCl, 30 mM imidazole, pH 8), and proteins were eluted through the column with a linear gradient to 100% of buffer B (20 mM Tris, 0.5 M NaCl, 0.5 M imidazole, pH 8). The purified His-tagged TasA protein was buffer exchanged using a PD-10 desalting column (GE Healthcare) equilibrated in TEV buffer (50 mM Tris-HCl (pH 8.0), 0.5 mM EDTA), followed by incubating with TEV protease (1 TEV: 50 TasA protein) at 30°C for 3 hours to cleave the His-tag. The TEV cleaved TasA was then eluted through the two stacked HisTrap Excel 5 mL columns in 20 mM Tris, 50 mM NaCl, pH 8, where the His-tag and TEV protein (containing its own His-tag) were retained on the column and the cleaved TasA eluted in the flow through. Protein concentration was determined from the absorbance measurement at 280 nm on a Nanovue spectrometer using the extinction coefficient for TasA of 14440 M^{-1} cm^{-1}. The mass of purified proteins was analysed using electrospray ionisation mass spectrometry (ESI-MS) at the Department of Chemistry, University of Cambridge.

Protein purity analysis by reversed phase chromatography

RP chromatography was carried out on a 1260 Infinity high-pressure liquid chromatography (HPLC) system (Agilent Technologies LDA UK Ltd.) to measure the purity of αS and TasA. 50 µL of sample was injected onto a Discovery BIOWide Pore C18 column (15 cm × 4.6 mm, 5 µm column with a guard column) (Supelco, Merck) and eluted with a gradient of 95% water and 0.1% acetic acid and 5% acetonitrile and 0.1% acetic acid to 5% water and 0.1% acetic acid and 95% acetonitrile and 0.1% acetic acid at a flow rate of 0.8 mL min^{-1} over 40 min. The elution profile was monitored by UV absorption at 220 and 280 nm. The area under the peaks in the chromatograph of absorption at 280 nm was calculated to provide the percentage purity. αS was 98% pure and TasA was 97% pure.

Protein aggregation

βLG (CAS 9045-23-2, Merck) powder was monomerised in hexa-iso-propanol (HFIP, Merck KGaA), before overnight lyophilisation (LyoQuest 85, Telstar, Spain). The freeze-dried monomers were dissolved in milli-Q water (MerckBurlington, MA, USA) to 100 µM. The mixture was then vortexed briefly and filtered through a 0.22 µm syringe filter (Millex-GS, Merck KGaA) to remove any clumps, before adjustment to pH2 using HCl (Merck, KGaA). Following this, the protein was aggregated at 80 °C for 3 hours on a ThermoMixer (Eppendorf, Hamburg, Germany). For storage, 0.05% of NaN_3 was added after βLG were formed. TasA was incubated at 70 µM at RT in 10 mM Tris pH 8 with 0.05% NaN_3 to prevent bacterial growth, rotating at 20 rpm (SB1, Stuart Scientific) for 1 week. αS was incubated at 100 µM in 10 mM Tris, or 140 mM KCl, 10 mM Tris pH 7.4 (mimicking intracellular conditions) or 140 mM NaCl, 1 mM CaCl2, 10 mM Tris (mimicking extracellular conditions) with 0.05% NaN_3 for 2 weeks at 37 °C rotating at 20 rpm on a (SB2, Stuart Scientific).

Circular dichroism (CD)

Protein samples were diluted to 2.5 µM and analysed in a 1mm cuvette at a temperature of 20°C. CD spectra were acquired using a JASCO J-810 spectropolarimeter (Jasco Inc, Easton, MD, USA). Spectra were recorded over the spectral range of 250 − 200 nm, with a resolution of 0.5 nm, a continuous scan at 50nm min^{-1}, and a bandwidth resolution of 1 nm. 10 accumulations were obtained for each sample and three preparations of each protein and buffer condition were measured. CD spectra of buffer only were recorded and subtracted from each sample spectrum. Mean residue ellipticity was calculated using **Equation 1**:

Equation 1

$$[\theta] = \frac{\theta_{obs}}{lcn}$$

where $[\theta]$ is the mean residue ellipticity (° cm^2 $dmol^{-1}$), θ_{obs} the observed ellipticity, l the path length (mm), c the molar concentration and n the number of residues (i.e., 140 amino acids (a.a.) for αS, 233 a.a. for TasA and 162 a.a. for βLG).

Fluorescence characterisation

Protein samples were loaded into a cuvette at 100 µM at room temperature, and placed into a spectrophotometer (F-4500, Hitachi, Tokyo, Japan). Excitation and emission spectra were captured by emission at 440 nm over a frequency

sweep between 280—420 nm (at 1 nm intervals), and excitation at 370 nm over 400—500 nm (at 1 nm intervals), respectively. Excitation and emission slits of 10 mm, and a scan speed of 240 nm min^{-1} were used. The fluorescence spectra of the buffer were measured at the same settings as the protein and subtracted from the final spectra. Measurements were based on triplicate measurements of three individual protein preparations. For the final plot, a MATLAB (MathWorks, Natick, MA, USA) script was used to identify the peak excitation and emission wavelengths and normalise the spectra across a range of 16 nm centred on the peak values.

Two-photon (2P-) fluorescence lifetime imaging microscopy (FLIM)

Samples at 100 μM were centrifuged and washed in dH_2O three times to remove salts. For HFIP treatment, 20 μL of HFIP (Merck KGaA) was added to 10 μL of 100 μM protein solution. After pipetting the sample to mix, the mixture was dried with a stream of N_2, before resuspension in 10 μL dH_2O. Protein samples were deposited onto a 1.5 thickness precision coverslip (Marienfeld GmbH, Lauda-Konigshofen, Germany) and dried on a hotplate for ~10 mins.

Samples were imaged on a home-built confocal fluorescence microscope equipped with a time-correlated single photon counting (TCSPC) module. A pulsed, femtosecond Ti:S laser (MaiTai DeepSee, SpectraPhysics, Oxford, UK) provided excitation at 740 nm and a repetition rate of 80 MHz. This was passed into a commercial microscope frame (IX83, Olympus, Tokyo, Japan) through a 60x oil objective (PlanApo 60XOSC2, 1.4 NA, Olympus). A bandpass filter of 450/50 (Chroma Technologies, Rockingham, VT, USA) was applied to the 2P emission to separate it from the excitation light. Laser scanning was performed using a galvanometric mirror system (Quadscanner, Aberrior, Gottingen, Germany). Emission photons were collected on a photon multiplier tube (PMT, PMC150, B&H GmBH, Berlin, Germany) and relayed to a time-corelated single photon counting card (SPC830, B&H GmBH). Images were acquired at 256x256 pixels for 200 s (i.e., 20 cycles of 10 s). Photon counts were kept below 1% of SYNC rates to prevent photon pile-up. TCSPC images were analysed using an in-house phasor plot analysis script (https://github.com/LAG-MNG-CambridgeUniversity/TCSPCPhasor), from which lifetime maps and phasor plots were generated. A general introduction to phasor plots is given in **Supplementary §1**.

Atomic force microscopy (AFM)

For imaging individual fibrils for morphological analysis, protein solutions were diluted to 10 μM in dH_2O, and incubated on poly-l-lysine (Merck KGaA) coated mica for 30 mins. To remove salts, the mica was washed thrice with dH_2O and dried under a gentle stream of N_2. The protein "meshes" corresponding to those imaged using 2P were prepared as described above. Imaging was performed on a BioScope Resolve (Bruker GmbH, Karlsruhe, Germany). The instrument was operated in ScanAsyst Air mode with a silicon nitride tip of a spring constant 40 N m^{-1} and nominal tip diameter of 2 nm (SCANASYST-AIR, Bruker). Images were collected at a scan rate of 1 Hz and resolution of 512x512 pixels.

Acquired AFM images were computationally flattened on Nanoscope Analysis 9.4 (Bruker GmBH) before import into MATLAB (MathWorks) using the MATLAB toolkit for Bruker. Batch analysis was performed using an in-house MATLAB script. A combination of manual and automatic segmentation of individual fibrils was performed. The height profile from each fibril was smoothed and characterised as either smooth or periodic as by a peak/trough search algorithm. For calculation of average fibril height, the mean across the whole fibril length and of the peaks

were used for smooth and periodic fibrils respectively. For periodic fibrils, the mean height of its peaks and troughs were additionally calculated.

Limited proteolysis of αS fibrils

100 μM of αS fibrils were incubated at 37°C in 3.8 μg mL^{-1} Proteinase K. 10 μL aliquots were removed at time points, 0, 1, 5 and 15 minutes and incubated with 20 mM PMSF to inactivate the proteinase K. The samples were frozen and lyophilised using a LyoQuest 85 freeze-dryer (Telstar, Spain). The protein films were solubilised in HFIP. HFIP was then evaporated under a stream of N_2 and the samples resuspended in LDS buffer before being heated to 100°C and analysed by SDS-PAGE on a 4-12% Bis-Tris gel (NuPAGE, Thermo Scientific) and stained with Coomassie blue (Merck KGaA).

Plotting and statistical analysis

All statistical analyses were performed on Prism 6 (GraphPad, San Diego, CA, USA), where a one-way ANOVA test with Holm-Sidak's multiple comparison was applied. Violin plots were produced using MATLAB (MathWorks) using open-source code from Anne Urai (github.com/anne-urai).

Supplementary Materials

Phasor plot analysis for 2P-FLIM

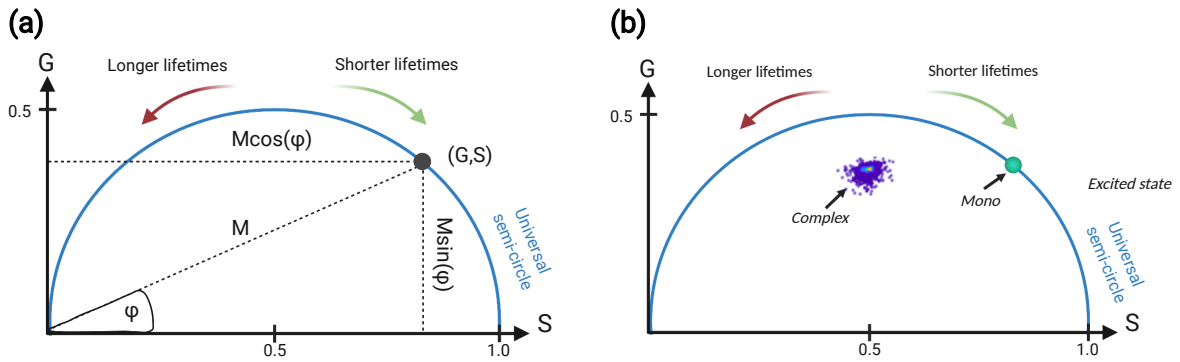

Supplementary Figure 1: Representative phasor plot. *(a) Time-domain TCSPC data can be Fourier-transformed into the frequency-domain (FD) and represented as 'phasors' with (G,S) coordinates on a polar plot (i.e., phasor plot). Analogous to FD-FLIM, resulting phasors have an associated phase (φ) and modulation (M), shifts in which indicate changes in fluorescence lifetimes. (b) Mono-exponential and complex exponential phasors fall on and within the universal semicircle respectively. Created on BioRender.com.*

Phasor plots are an efficient way to represent complex exponential decay fluorescence lifetimes.[23,25,45] It is a model-free, global representation of fluorescence lifetime data, which clearly shows how ensemble image pixels are affected by the chemical, physical and environmental changes of the sample. It stems from frequency-domain (FD-)FLIM where an intensity modulated light source is used to excite the sample, and the demodulation and phase shift in the resulting fluorescence emission is measured. Hence, the phase angle (φ) and modulation (M) for each pixel within the image can be conveniently represented on a phasor plot, with real and complex coordinates, (G,S).[23,25,45,46] For use with time-domain time-correlated single photon counting (TCSPC) data, a Fourier transform is required. The exponential decays of each of the 256 time bins, along each 256 by 256 x- and y-coordinates of the TCSPC image is represented as a single plot (i.e., 'phasor') within the plot (**Supplementary Figure 1a**), with (G,S) calculated as follows:

Equation 2

$$G(\omega) = \frac{\int_0^\infty I(t)\cos(\omega t)\,dt}{\int_0^\infty I(t)dt}$$

Equation 3

$$S(\omega) = \frac{\int_0^\infty I(t)\sin(\omega t)\,dt}{\int_0^\infty I(t)dt}$$

where $\omega = 2\pi f$ is the laser repetition angular frequency, f is the laser repetition rate, I is fluorescence intensity (i.e. total number of photons) and t is time. The phasor plot has a universal semicircle, which represents mono-exponential decay lifetimes (**Equation 4, Supplementary Figure 1b**):

Equation 4

$$(G(\omega) - 0.5)^2 + S(\omega)^2 = 0.25$$

This is dependent on ω, hence scales with f. Calibration of the phasor plot was performed using standard fluorescence dyes of known mono-exponential fluorescence lifetimes, i.e., Coumarin 6 (Merck KGaA) in ethanol. Multi-exponential species (e.g., intrinsic amyloid fluorescence) have phasors lying within the universal semicircle (**Supplementary Figure 1b**). An independent determination of fluorescence lifetime as modulation (τ_M, **Equation 5**) and phase (τ_ϕ, **Equation 6**) can be made:

Equation 5

$$\tau_\phi = \frac{S(\omega)}{\omega\, G(\omega)}$$

Equation 6

$$\tau_M = \frac{1}{\omega}\sqrt{\frac{\cos(\phi)^2}{G(\omega)^2} - 1} = \frac{1}{\omega}\sqrt{\frac{\sin(\phi)^2}{S(\omega)^2} - 1}$$

where $\phi = \tan^{-1}\left(\frac{S}{G}\right)$ is the phase.

For purposes of comparison in the manuscript, τ_M (i.e., more sensitive to changes in G) is used over τ_ϕ (i.e., more sensitive to changes in S) as it is the more sensitive fluorescence lifetime for changes between different amyloid/polymorph samples.

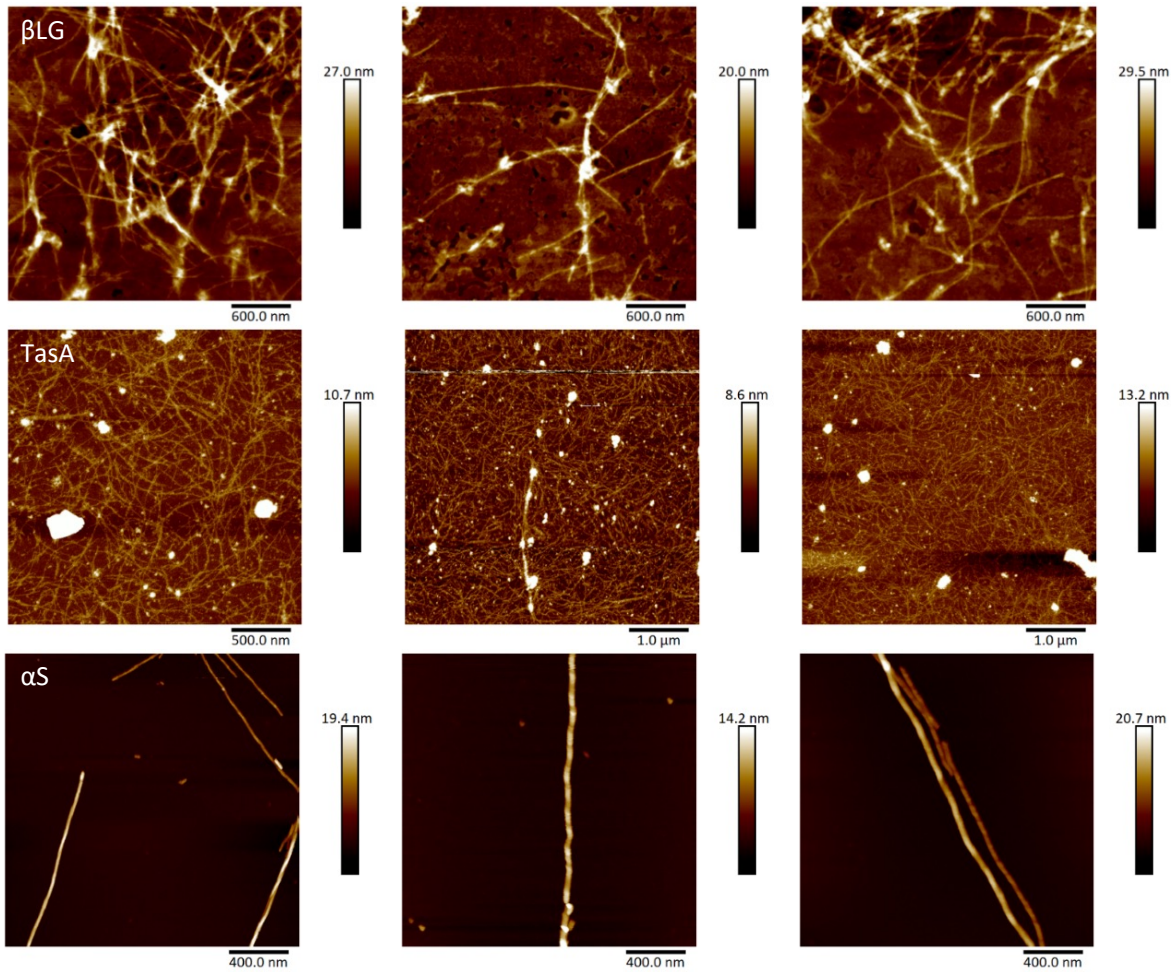

Supplementary Figure 2: βLG, TasA and αS feature different fibril morphologies. *Representative AFM images of 10 µM of each protein. βLG and TasA have no/less periodicity compared to αS fibrils. TasA fibrils are very thin in comparison to βLG and αS. Height profile is shown in brown scale.*

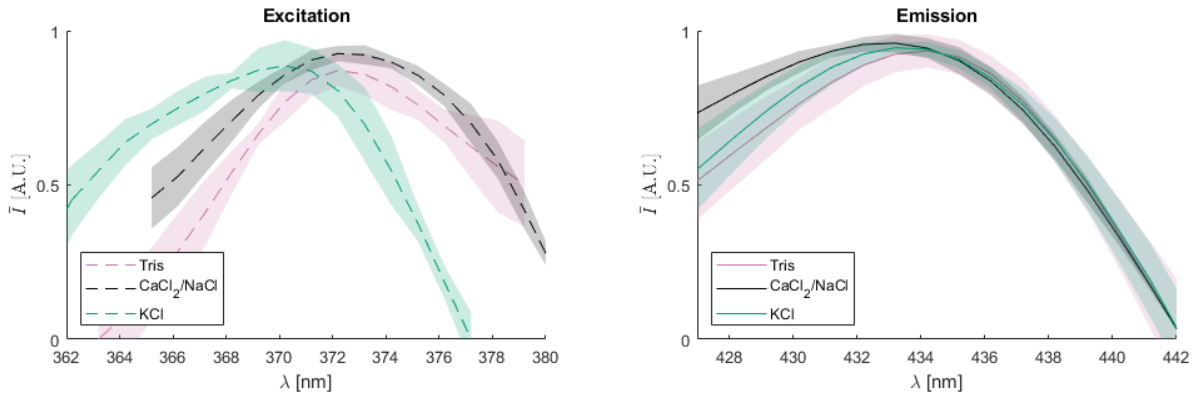

Supplementary Figure 3: αS aggregated in different salt buffers have similar excitation and emission profiles. *(a) Excitation and emission spectra were measured between 340 to 400 nm with the emission set at peak emission, and emission spectra were measured between 400 to 460 nm with the excitation set at peak excitation for each protein. Excitation and emission peaks for each protein were: Tris – ex 373 nm, em 433 nm, $CaCl_2$/NaCl – ex 373 nm, em 433 nm, and KCl – 370 nm, em 432 nm. Displayed are the average of three scans from three individual protein preparations.*

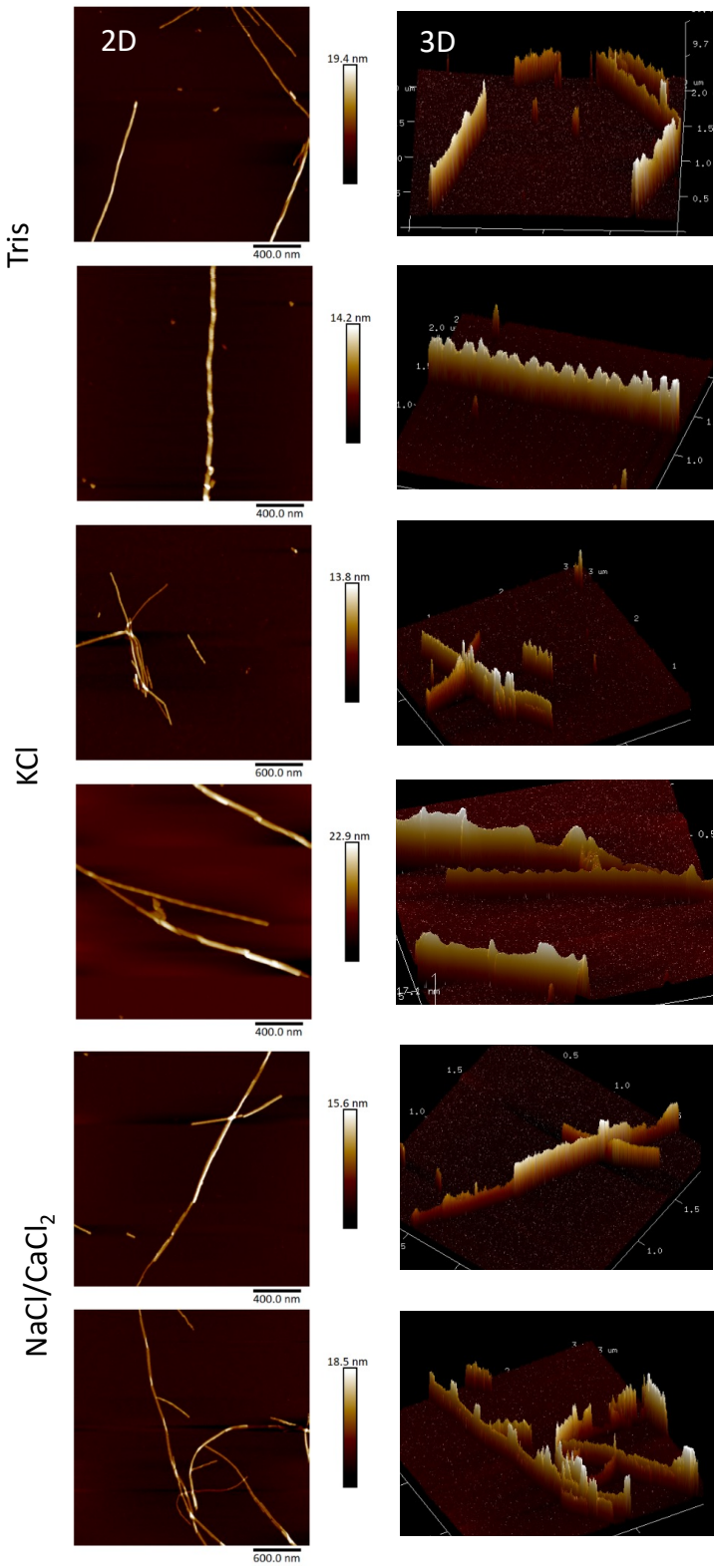

Supplementary Figure 4: Different fibril polymorphs are observed for aSyn in different buffers. *Representative AFM images of 5 µM aS in 20 mM Tris pH 7.4, with additional KCl (140 mM) or NaCl (140 mM) and $CaCl_2$ (1 mM) on freshly cleaved mica. 2D images on the left show the height profile of fibrils. The 3D images on the right more clearly show periodicity of the fibrils.*

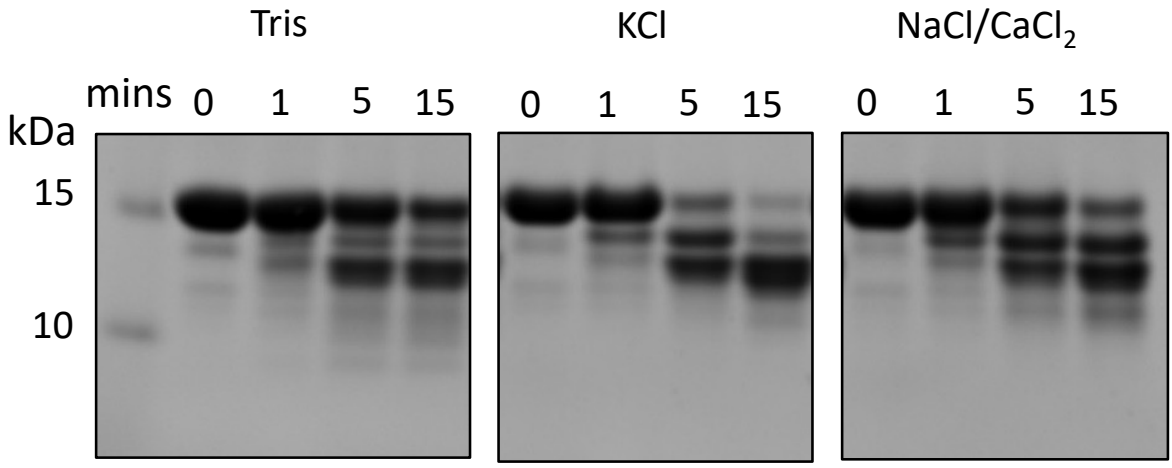

Supplementary Figure 5. Repeated limited proteolysis profiles of αS fibrils shows reproducibility in digestion profiles. *100 μM of aS in each buffer condition was incubated in 3.8 μg/ml proteinase K for 0, 1, 5 and 15 mins. Monomeric aS is ~14.4 kDa, degradation patterns of the three samples show a similar band profile, but the intensities differ, indicating differences in cleavage rates. This repeat has similar proteolysis profiles to* ***Figure 4****, showing reproducible results.*